

## Supporting information

### Thermal Behavior

The thermal properties of crystals I-IV were investigated by DSC and TGA experiments (Figure 1S). Crystal I shows only one endothermic peak at 214 °C (onset temperature: 211 °C) in its DSC pattern. In addition, TGA experiment indicates that the weight loss begins at around 214 °C, suggesting that APAP melts with concomitant decomposition.

Crystal II shows two endothermic peaks at 102 and 213 °C and the TGA analysis suggests it loses weight in two steps. The first endotherm at 102 °C is ascribed to the removal of chloroform molecules and the weight loss (24.11 %) from 80 to 120 °C also coincides with the expected weight loss of 24.67% corresponding to the 1:1 APAP·chloroform system. The second endotherm and the second step of weight loss are in agreement with that of crystal I, and analysis of PXRD pattern of the residue after desolvation (Figure 2S) revealed that it also matched with crystal I, indicating the residue possesses the same structure with crystal I.

Similarly, crystal III also shows two endothermic peaks and two steps of weight loss. The first endotherm at 138 °C is ascribed to the removal of phenol molecules, and the weight loss (20.24 %) from 80 to 145 °C also coincides with the expected weight loss of 20.52 % corresponding to the 1:1 APAP·phenol system. The other changes in DSC and TGA curves are also in agreement with that of crystal I, indicating the same phase is obtained after removal of phenol.

However, crystal IV shows a broad endothermic peak at 221 °C, which is different from the two starting components, suggesting the formation of a new phase. Moreover, the TGA curve indicates the weight loss begins before appearance of the endothermic peak, which may be relative to the low melting point and thermal stability of BPA.

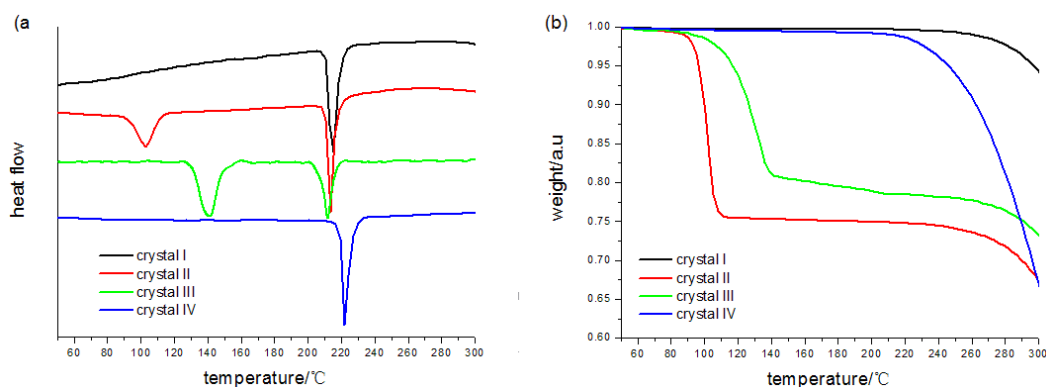


**Figure 1S.** DSC (a) and TGA (b) profiles of crystals I-IV.

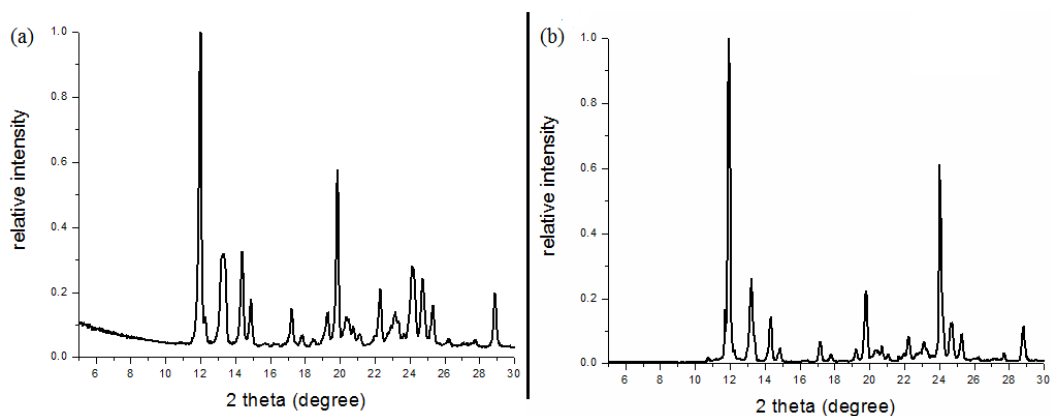


**Figure 2S.** PXRD patterns of the residue (a) and crystal I (b).

### FT-IR Spectroscopy

To investigate the non-covalent interactions within these crystals, their FT-IR spectra were recorded (Figure 3S). For the carbonyl groups of APAP, the vibrational absorption maximum in crystals I-IV are 1666, 1648, 1633 and 1627  $\text{cm}^{-1}$ , respectively. This result indicates that the different strength of intermolecular C-H $\cdots$ O or O-H $\cdots$ O hydrogen bonding interactions between APAP and the guest molecules exert different influence on the vibrational properties of APAP. For our system, with decrease of the distance between the hydrogen atom and acceptor (H $\cdots$ A, Table 2), the values are shifted to lower frequencies.

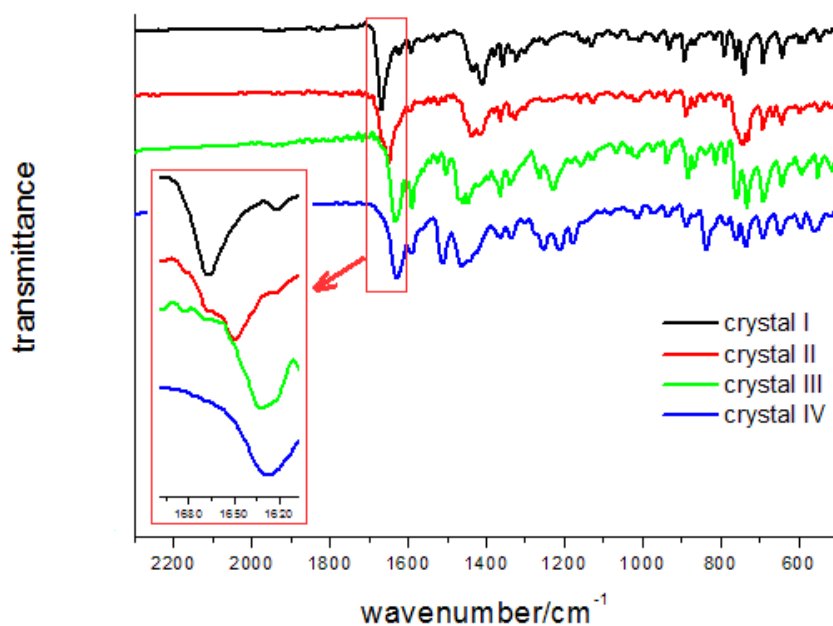


**Figure 3S.** FT-IR spectra of crystals I-IV.

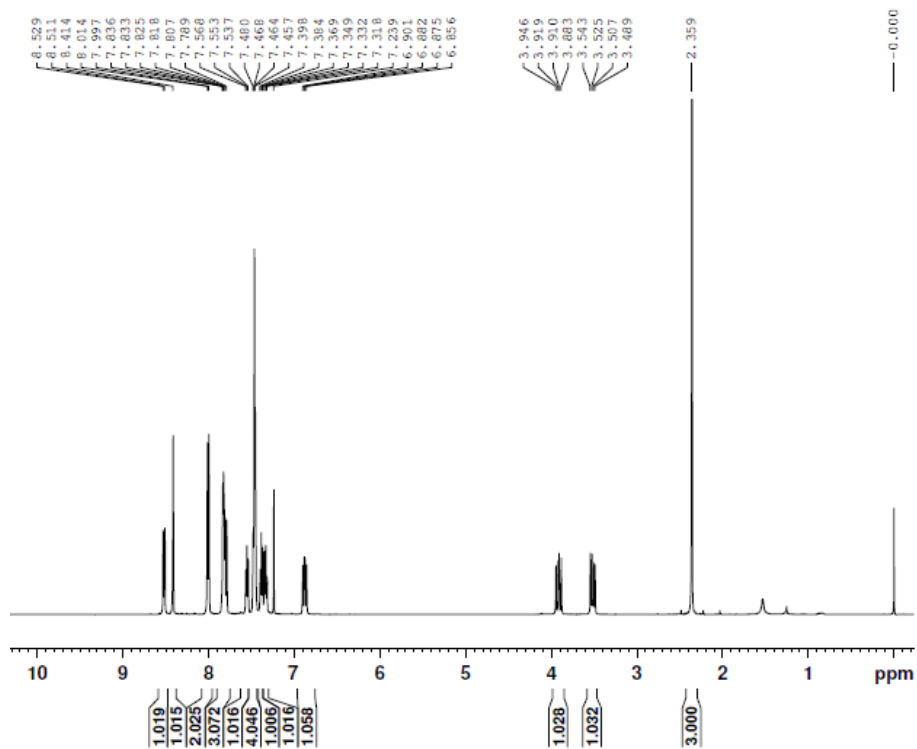


**Figure 4S.** <sup>1</sup>H NMR spectrum of APAP.

Assignments of each H in the NMR spectrum:  $\delta$  (ppm) 2.35 (CO-CH<sub>3</sub>), 3.48-3.54 (one H of CH<sub>2</sub>), 3.88-3.94 (another H of CH<sub>2</sub>), 6.85-6.90 (CH), 7.31-8.52 (14H, Ar-H from anthracne and benzene rings).

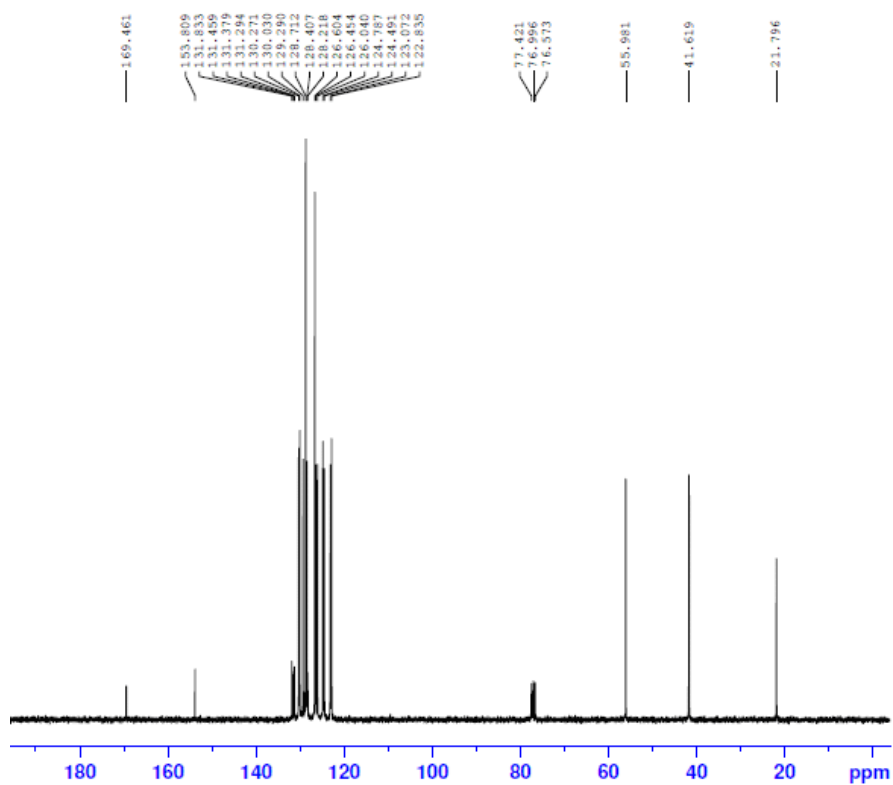


**Figure 5S.**  $^{13}\text{C}$  NMR spectrum of APAP

Assignments of C in the NMR spectrum:  $\delta$  (ppm) 21.79 ( $\text{C}^*-\text{CO}$ ), 41.61 ( $\text{CH}_2$ ), 55.98 ( $\text{CH}-\text{N}$ ), 122.83-131.83 (the rest Ar-C from pyrene and benzene rings), 153.80 ( $\text{C}=\text{N}$ ), 169.46 ( $\text{C}=\text{O}$ ). (21.79 is assigned to  $\text{C}^*$ ).

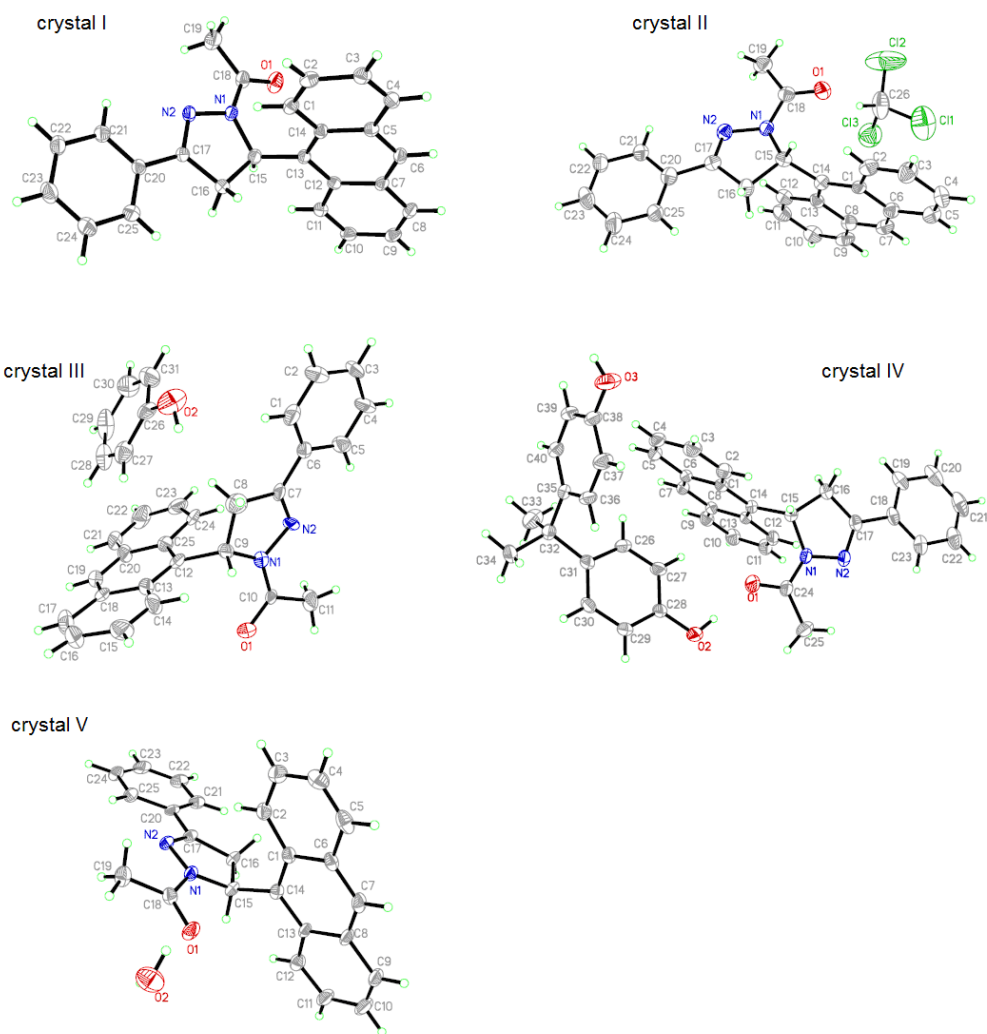


**Figure 6S .** Thermal ellipsoid plots of crystals I-V at 20% probability.

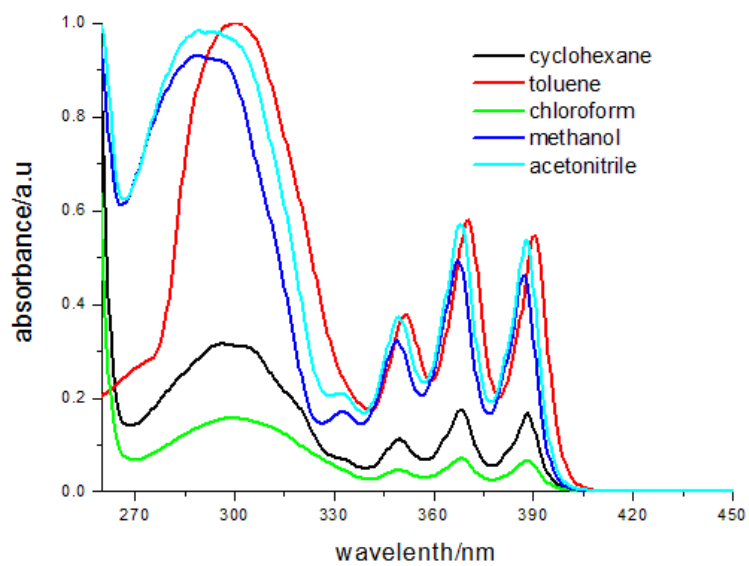


**Figure 7S** . UV-Vis spectra of APAP in various solvents.

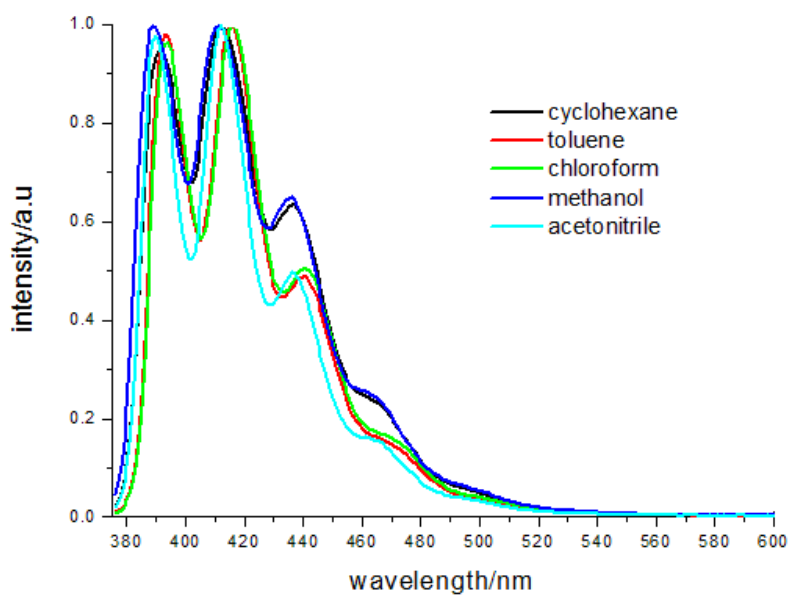


**Figure 8S**. Fluorescence spectra of APAP in various solvents ( $\lambda_{ex}=365$  nm).

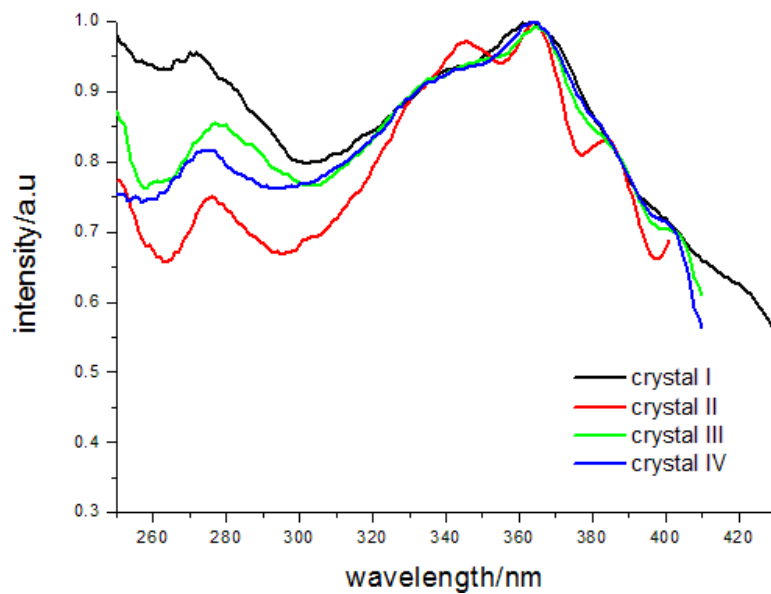


**Figure 9S.** Excitation spectra for crystals I-IV.

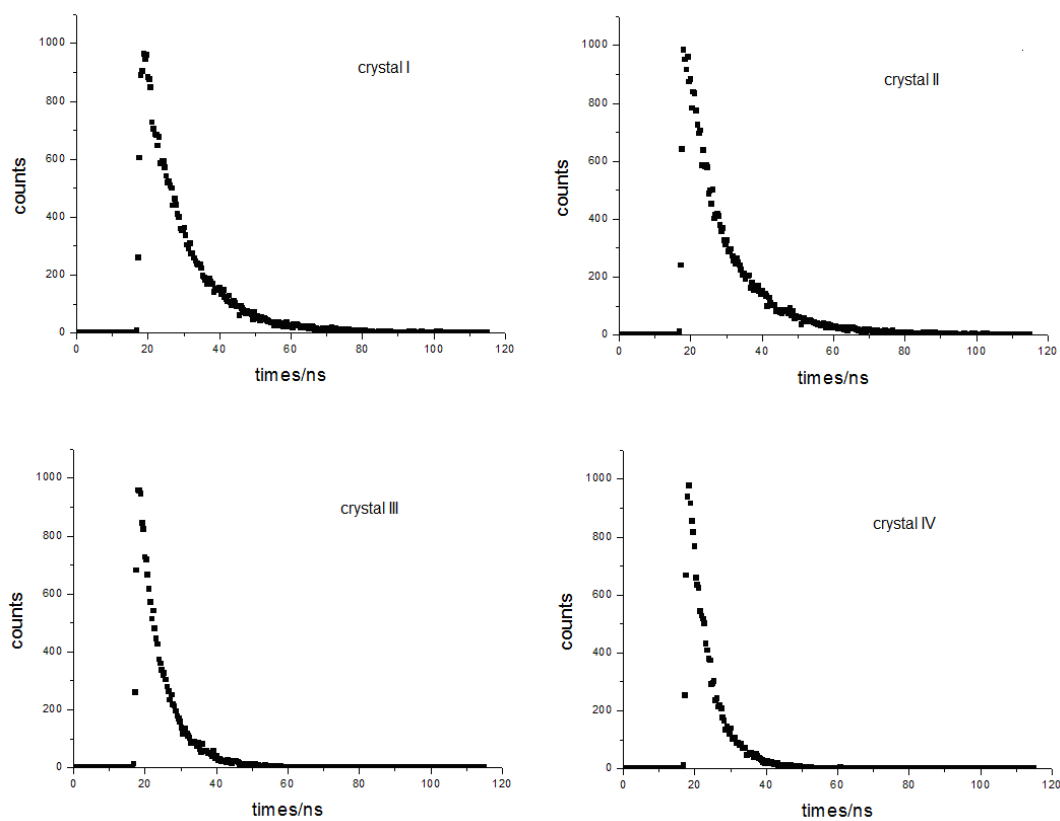


**Figure 10S.** Fluorescence decay curves for crystals I-IV (fluorescence lifetimes were monitored at 340 nm).

**Table 1S.** Intermolecular hydrogen bonds parameters in crystals I-V.

crystal	D-H (Å)	H···A (Å)	D···A (Å)	∠D-H···A (°)
II				
C26-H26A···O1	0.98	2.09	3.040(6)	161.70
III				
O2-H2C···O1	0.82	1.91	2.727(8)	174.40
C8-H8B···O1	0.97	2.43	3.272(10)	145.49
IV				
O2-H2C···O1	0.82	1.82	2.640(3)	177.33
O3-H3B···O2	0.82	1.87	2.646(4)	158.69
C2-H2B···O3	0.93	2.43	3.235(5)	144.97
C27-H27A···O1	0.93	2.52	3.190(4)	128.84
V				
O2-H2B···O1	0.85	2.41	2.800(4)	108.71
O2-H2C···O1	0.85	2.43	2.800(4)	106.79

**Table 2S.**  $\pi$ - $\pi$ , C-H··· $\pi$  and C-Cl··· $\pi$  interactions in the crystals I-V.

crystal	interaction	distance (Å) <sup>[a]</sup>	distance (Å) <sup>[b]</sup>	Angle (°) <sup>[c]</sup>
I				
	anthracene···anthracene <sup>[d]</sup>	5.414	3.232	0
II				
	C19-H19B···anthracene	2.88		152
	C2-H2A···anthracene	3.04		154
	C26-Cl1···anthracene	3.913(3)		84.7(2)
	C26-Cl3···anthracene	3.822(3)		104.4(2)
III				
	C28-H28A···anthracene	2.98		120
	C14-H14A···anthracene	2.97		147
	benzene···anthracene	3.908(5)		11.4(4)
IV				
	C26-H26A···anthracene	3.00		132
	C30-H30A···anthracene	2.96		132
	C11-H11A···benzene	2.70		152
	C34-H34C···anthracene	2.63		156
V				
	C19-H19B···anthracene	2.88		153
	benzene···benzene	3.920(2)	3.354(3)	0

[a] The distances were measured from the centre to the centre of the aromatic rings (for  $\pi$ - $\pi$  interactions) or from hydrogen atom to the centre of the aromatic ring (for C-H··· $\pi$  interaction); [b] interplanar separation between the aromatic rings (for  $\pi$ - $\pi$  interactions); [c] The angles were measured between the planes of the aromatic rings (for  $\pi$ - $\pi$  interactions) and C-H···centre (for C-H··· $\pi$  interaction); [d] is the whole anthracene ring, the rest is one six-membered ring of the anthracene.